THE UNIVERSITY of EDINBURGH

Edinburgh Research Explorer

Quantitative proteomics of the mitotic chromosome scaffold reveals the association of BAZ1B with chromosomal axes

Citation for published version:
Ohta, S, Taniguchi, T, Sato, N, Hamada, M, Taniguchi, H & Rappsilber, J 2019, 'Quantitative proteomics of the mitotic chromosome scaffold reveals the association of BAZ1B with chromosomal axes' Molecular and Cellular Proteomics, vol. 18, no. 2, pp. 169-181. DOI: 10.1074/mcp.RA118.000923

Digital Object Identifier (DOI):
10.1074/mcp.RA118.000923

Link:
Link to publication record in Edinburgh Research Explorer

Document Version:
Peer reviewed version

Published In:
Molecular and Cellular Proteomics

General rights
Copyright for the publications made accessible via the Edinburgh Research Explorer is retained by the author(s) and / or other copyright owners and it is a condition of accessing these publications that users recognise and abide by the legal requirements associated with these rights.

Take down policy
The University of Edinburgh has made every reasonable effort to ensure that Edinburgh Research Explorer content complies with UK legislation. If you believe that the public display of this file breaches copyright please contact openaccess@ed.ac.uk providing details, and we will remove access to the work immediately and investigate your claim.

OPEN ACCESS

Download date: 07. Aug. 2019

Quantitative proteomics of the mitotic chromosome scaffold reveals the association of BAZ1B with chromosomal axes

Shinya Ohta[1]*, Takako Taniguchi[2], Nobuko Sato[1], Mayako Hamada[1], Hisaaki Taniguchi[2], and Juri Rappsilber[3, 4]

[1]Medical School, Kochi University
Kohasu, Oko-cho, Nankoku, Kochi 783-8505, JAPAN

[2]Institute for Enzyme Research, Tokushima University
3-18-15 Kuramoto-cho, Tokushima, 770-8503, JAPAN

[3]Bioanalytics, Institute of Biotechnology, Technische Universität Berlin, 13355 Berlin, Germany

[4]Wellcome Centre for Cell Biology, School of Biological Sciences, University of Edinburgh, Max Born Crescent, Edinburgh EH9 3BF, UK

*Corresponding author
E mail: shinya.ohta@kochi-u.ac.jp
Phone: +81-(0)88-880-2309

Running title: Quantitative proteomics of the mitotic chromosome scaffold

Abbreviations: BAZ1A, bromodomain adjacent to zinc-finger 1A; BAZ1B, bromodomain adjacent to zinc-finger 1B; CAP-G, chromosome-associated protein G; DSB, DNA double-strand break; FBS, fetal bovine serum; FW, forward; HAMMOC, hydroxy acid-modified metal oxide chromatography; GAPDH, glyceraldehyde 3-phosphate dehydrogenase; GFP, green fluorescent protein; IMS, intrinsic metaphase structure; ISWI, imitation switch; KIF4A, kinesin family member 4A; KO, knock out; NEB, nuclear envelope breakdown; PTS, phase-transfer surfactant; RV, reverse; SILAC, stable isotope labeling with amino acids in cell culture; SMARCA5, SWI/SNF-related matrix-associated actin-dependent regulator of chromatin subfamily A member 5; SMC2, structural maintenance of chromosomes protein 2; SNF, sucrose non-fermenting protein; TOP2A, DNA topoisomerase IIα; WSTF, William syndrome transcription factor; WT, wild type

Quantitative proteomics of the mitotic chromosome scaffold

Summary

In mitosis, chromosomes achieve their characteristic shape through condensation, an essential process for proper segregation of the genome during cell division. A classical model for mitotic chromosome condensation proposes that non-histone proteins act as a structural framework called the chromosome scaffold. The components of the chromosome scaffold, such as DNA topoisomerase IIα (TOP2A) and structural maintenance of chromosomes protein 2 (SMC2), are necessary to generate stable mitotic chromosomes; however, the existence of this scaffold remains controversial. The aim of this study was to determine the protein composition of the chromosome scaffold. We used the DT40 chicken cell line to isolate mitotic chromosomes and extract the associated protein fraction, which could contain the chromosome scaffold. MS revealed a novel component of the chromosome scaffold, bromodomain adjacent to zinc finger 1B (BAZ1B), which was localized to the mitotic chromosome axis. Knocking out BAZ1B caused prophase delay due to altered chromosome condensation timing and mitosis progression errors, and the effect was aggravated if BAZ1A, a BAZ1B homolog, was simultaneously knocked out; however, protein composition of

prometaphase chromosomes was normal. Our results suggest that BAZ1 proteins are essential for timely chromosome condensation at mitosis entry. Further characterization of the functional role of BAZ1 proteins would provide new insights into the timing of chromosome condensation.

Quantitative proteomics of the mitotic chromosome scaffold

Introduction

A major challenge in the field of mitosis research is elucidation of the mechanism through which chromosomes achieve the necessary 10,000-fold shortening of DNA and thus acquire the characteristic structure essential for proper mitosis. A classical model proposes that non-histone proteins act as a structural framework during the formation of mitotic chromosomes (1). This "chromosome scaffold" was hypothesized to be an insoluble biochemical fraction that could be obtained from chromosomes after most of the DNA and proteins were solubilized (2). The major components of this fraction are structural maintenance of chromosomes protein 2 (SMC2) and DNA topoisomerase IIα (TOP2A) (3), which is thought to affect chromosome condensation during late mitosis (4, 5).

A breakthrough in understanding of the chromosome condensation mechanism was the identification of condensin, a pentameric protein complex including SMC2 (6-8). The purified chromatin-associated protein complex from *Xenopus* egg extracts, which contains chromosome-associated protein (CAP)-E/SMC2, CAP-C/SMC4, CAP-D2, CAP-G, and CAP-H, showed chromosome condensation activity

in vitro (6, 9) by introducing positive supercoils into relaxed plasmid DNA in the presence of topoisomerase I (9). Furthermore, it has been shown that the condensin complex localizes on the mitotic chromosome axis in many vertebrate species (10, 11).

When the second condensin complex (condensin II: SMC2, SMC4, CAP-D3, CAP-G2, and CAP-H2) was discovered, the canonical condensin complex was retroactively named condensin I (12). Both condensin complexes localize to the mitotic chromosome axis but show alternate distribution (12, 13). Thus, condensin II exists predominantly in the nucleus during interphase, whereas condensin I is sequestered in the cytoplasm and gains access to chromosomes only after nuclear envelope breakdown (NEB) in prometaphase (13). These findings suggest that the two condensin complexes act sequentially to initiate the assembly of mitotic chromosomes (14, 15). Condensin II is involved in DNA repair during interphase through association with several chromosomal proteins and chromosome condensation during mitotic entry (13, 16). Moreover, TOP2A and kinesin family member 4A (KIF4A), both included in the chromosome scaffold fraction, show alternate localization on the mitotic chromosome axis (17, 18). However, the existence

and functional significance of such a chromosome scaffold is highly controversial, and another widely accepted model proposes that chromosomes are formed solely through a hierarchy of chromatin coiling events (19).

Several studies have demonstrated the involvement of bromodomain adjacent to zinc finger 1B (BAZ1B) in heterochromatin remodeling (20, 21). The gene encoding BAZ1B is also known as the William syndrome transcription factor (WSTF) because of its initial identification as a hemizygously deleted gene in patients with the disease (22). BAZ1B may form a complex with the nucleosome-dependent ATPase, imitation switch (ISWI)/sucrose non-fermenting protein (SNF)-related matrix-associated actin-dependent regulator of chromatin subfamily A member 5 (SMARCA5) (20, 21). BAZ1B depletion was reported to affect the localization of heterochromatin protein 1 (HP1) and histone H3 with trimethylated lysine-9 (HH3-K9me3) (23). Furthermore, BAZ1B exhibits tyrosine-protein kinase activity during DNA double-strand break (DSB) repair by phosphorylating Tyr-142 on histone H2A.X (HH2A.X-pY142 or γ-H2A.X), a protein that recruits the MRN complex, including Mre11, Rad50, and Nbs1, during initial DSB processing (24, 25). Moreover, it has now become clear

that BAZ1B forms a complex with topoisomerase I and SMARCA5 during the S phase and is associated with the progression of DNA replication forks (26).

In addition, the human genome contains the *BAZ1A* gene (also named ATP-utilizing chromatin assembly factor 1, *ACF1*), which encodes a protein showing 21% amino-acid sequence homology with BAZ1B. Similar to BAZ1B, BAZ1A interacts with SMARCA5 to form the chromatin accessibility complex (CHRAC), which is required for DSB repair through recruitment of Ku proteins in human cells (27). Moreover, BAZ1A and BAZ1B were identified in mitotic chromosomes assembled in *Xenopus* egg extracts (14, 28). However, the functions of both BAZ1A and BAZ1B in mitosis remain unclear.

In this study, we used MS to determine the protein composition of the chromosome scaffold in chicken DT40 cells. To our knowledge, this is the first quantitative proteomic analysis showing that BAZ1B is present in the mitotic chromosome scaffold along with previously identified components such as TOP2A, SMC2, and KIF4A. Our results suggest that BAZ1B and its homolog BAZ1A co-regulate the timing of chromosomal condensation prior to mitotic entry.

Experimental Procedures

Cell culture

Chicken DT-40 cells (clone 18) were maintained in Roswell Park Memorial Institute (RPMI) 1640 medium (Wako Pure Chemical Industries Ltd., Osaka, Japan) supplemented with 10% (v/v) fetal bovine serum (FBS), 1% chicken serum, 100 U/mL penicillin, and 100 μg/mL streptomycin (Wako Pure Chemical Industries Ltd.) at 39°C and 5% CO_2 in a humidified incubator. For ^{13}C and ^{15}N labeling of lysine and arginine, cells were maintained at 37°C in L-lysine/L-arginine-free RPMI (Thermo Fisher Scientific, Waltham, MA, USA) supplemented with 10% (v/v) FBS (Thermo Fisher Scientific) dialyzed through a 10,000-molecular-weight cut-off filter, 100 μg/mL U-$^{13}C6^{15}N2$-L-lysine:2HCl, 30 μg/mL U-$^{13}C6^{15}N4$-L-arginine:HCl, 100 U/mL penicillin, and 100 μg /mL streptomycin (Wako Pure Chemical Industries Ltd.). To obtain $SMC2^{OFF}$ cells, $SMC2^{ON/OFF}$ cells were grown in the presence of doxycycline for 30 h prior to blocking with nocodazole to inhibit SMC2 expression (11).

U2OS or HeLa (Kyoto) cells in the exponential growth phase were seeded

onto coverslips and grown overnight at 37°C and 5% CO_2 in Dulbecco's Modified Eagle medium (DMEM, Wako Pure Chemical Industries Ltd.) supplemented with 10% FBS, 100 U/mL penicillin, and 100 μg/mL streptomycin.

Isolation of mitotic chromosomes

DT40 and HeLa cells were incubated with 0.5 μg/mL nocodazole for 13 and 24 h, respectively, resulting in a mitotic index of 70–90%. Cells were swollen in hypotonic buffer containing 40 mM KCl for 5 min and disrupted in polyamine-EDTA buffer containing 0.75 mM spermidine, 0.3 mM spermine, 2 mM K-EDTA (pH 7.4) (Sigma-Aldrich, St. Louis, MO, USA), and 0.1% digitonin (Biosynth, Staad, Switzerland) using a 15-mL Dounce homogenizer (2, 29, 30). Mitotic chromosomes were purified by density gradient centrifugation in sucrose (15%, 60%, and 80%) and then in Percoll (GE Healthcare Ltd., Buckinghamshire, UK). All buffers used contained 1 μg/mL antipain, 1 μg/mL chymostatin, 1 μg/mL leupeptin, 1 μg/mL pepstatin A (Peptide Institute, Inc., Osaka, Japan), 1 μg/mL aprotinin, 0.1 mM phenylmethylsulfonyl fluoride (Wako Pure Chemical Industries Ltd.), and phosphatase

inhibitor cocktails 2 and 3 (1:1,000; Sigma-Aldrich).

Mitotic chromosomes from three independent preparations were pooled together and solubilized in phase-transfer surfactant (PTS) buffer (31).

Isolation of histone-depleted mitotic chromosomes

Histone-depleted mitotic chromosomes were prepared as previously described (2, 29) and transferred to non-EDTA polyamine buffer containing 0.375 mM spermidine and 0.03% N,N-dimethyldodecylamine N-oxide. DNA was digested by adding 40 μg/mL micrococcal nuclease and 2 mM calcium chloride for 20 min. Chromosomes were treated with 0.1 mM copper sulfate under nitrogen gas flow for 10 min and diluted with an equal volume of 1× TEE buffer (1 mM triethanolamine-HCl, pH 8.5, and 0.2 mM Na-EDTA). An equal volume of 2× lysis buffer (20 mM Tris-HCl, pH 9.0, 20 mM Na-EDTA, 0.06% N,N-dimethyldodecylamine N-oxide, and 4 M NaCl) was immediately added, and the mixture was incubated for 20 min. The histone-depleted mitotic fraction was obtained in the pellet after centrifugation at 10,000 × *g* for 5 min.

Quantitative proteomics of the mitotic chromosome scaffold

Histone-depleted mitotic chromosomes isolated from mitotic DT40 cells grown in heavy SILAC medium were mixed with an equal amount (w/w) of a "mimic" histone-depleted mitotic chromosome fraction isolated from a parallel culture in light SILAC medium using 1% β-mercaptoethanol, which disrupts the chromosome scaffold, resulting in the purification of the background fraction (2, 29). This procedure enabled us to perform quantitative comparison between the histone-depleted mitotic chromosome fraction and the background because it removed many contaminants from the list of potential chromosome scaffold proteins (Fig. S1A).

Trypsin digestion

Proteins associated with mitotic chromosomes were extracted using PTS (32), and 100-μg aliquots were digested with 1 μg endoproteinase Lys-C (Wako Pure Chemical Industries Ltd.) and 0.4 μg trypsin (Promega, Fitchburg, WI, USA) in 2 mM DTT and 10 mM IAA for 16 h. Digestion was stopped with 1% trifluoroacetic acid followed by desalting with an SDB-XC StageTip (33).

Mass spectrometry

The digested peptides or enriched phosphopeptides were analyzed on a Q Exactive Hybrid Quadrupole-Orbitrap Mass Spectrometer or an Orbitrap Fusion Tribrid Mass Spectrometer (Thermo Fisher Scientific, Bremen, Germany) using the acquisition software for the fusion. MS2 spectra were obtained using the Orbitrap analyzer on the Orbitrap Fusion Mass Spectrometer. For LC-MS/MS analysis, we used a Dionex μ-Precolumn (5 μm particle size, 300 μm inner diameter × 5 mm length) and an Acclaim PepMap100 C18 separation column (3 μm particle size, 75 μm inner diameter × 150 mm length) as described in a previous report (34). Peptides were eluted with a nonlinear gradient of 4–30% buffer B (0.2 % formic acid [FA], 5% DMSO in acetonitrile) in buffer A (0.2% FA, 5% DMSO in double-distilled water) applied at a flow rate of 250 nL/min over 123 min. After each elution, the column was washed with 96% buffer B and re-equilibrated with buffer A. All parameters used in MS analysis are shown in Table S1.

Peptide identification and quantification

Quantitative proteomics of the mitotic chromosome scaffold

For identification of proteins and phosphorylation sites, peak lists were created using Andromeda (35) based on recorded fragmentation spectra searched against the *Gallus gallus* protein database in UniProt (release 2013_07) and our in-house chicken database. Spectra were also searched against the *Homo sapiens* protein database in UniProt (release 2016_11). Precursor mass tolerance was 10 ppm, fragment ion mass tolerance was 0.02 Da, and trypsin specificity was strict (C-terminal cleavage of Lys or Arg but not before Pro), allowing up to four missed cleavages. The results of stable isotope labeling with amino acids in cell culture (SILAC) were quantified using MaxQuant 1.4.0.3 or 1.5.6.5. Details of the parameters are given in Table S2. MS proteomic data and all other parameters used in MaxQuant have been deposited in the ProteomeXchange Consortium (http://proteomecentral.proteomexchange.org) via the JPOST partner repository (dataset identifiers: PXD007269, PXD008429, and PXD008696) (36-38). All protein and phosphopeptide quantification data are also presented in Tables S3–S7.

Plasmid construction

Quantitative proteomics of the mitotic chromosome scaffold

The ORFs of human *BAZ1A* and *BAZ1B* were amplified by PCR from total cell RNA using Superscript II and KOD polymerase and inserted into the entry vector (pENTR™ 4 Dual Selection Vector; Thermo Fisher Scientific) between *Xmn*I and *Not*I sites. Vectors for overexpression in human cells were generated via LR clonase-mediated recombination between the entry vector and pDEST131NGFP (39). The pTORA14BAZ1A plasmid for CRISPR-mediated mutagenesis was obtained by inserting the double-strand oligo DNA fragment into the *Age*I site (blunted by Mung Bean Nuclease) of pTORA14 constructed from the U6gRNA-Cas9-2A-GFP plasmid (CAS9GFPP-1EA, Sigma-Aldrich). The guide RNA target sequence in the DNA fragment was 5′-TCTGTCTCACAAACGGCTTT-3′.

CRISPR-mediated mutagenesis

HeLa cells were transfected with pTORA14BAZ1A or the SIGMA CRISPR plasmid for BAZ1B (guide RNA target sequence 5′-GTGAAGCCGTTGCCCGGAG-3′; HS0000488765, Sigma-Aldrich) and sorted based on GFP intensity in a FACSAria II flow cytometer (Becton Dickinson, Franklin Lakes, NJ, USA). To extract genomic DNA,

sorted cells were resuspended in lysis buffer (50 mM KCl, 10 mM Tris-HCl, pH 9.0, 0.1% Triton-X 100, 0.4 mg/mL proteinase K) and incubated at 50°C for 3 h. Loci targeted by guide RNAs were amplified and sequenced using the following primers: forward: 5′-CAGGACGAGAGGAGGTAGGG-3′ and reverse: 5′-TACCAACCCGCGTTCCCCAC-3′ for BAZ1A KO;

forward: 5′-AATAATTTCCTCCGGTGCTG-3′ and reverse: 5′-TCCTCAAGGCCTAAAGCCAAC-3′ for BAZ1B KO. Sequence traces were analyzed by tracking indels by decomposition (TIDE) (40).

Immunoblotting

Proteins were analyzed using the following rabbit primary antibodies: anti-SMC2 at 1:500 (11), anti-chicken TOP2A at 1:1,000 (41), and anti-BAZ1A at 1:500 (ab15826; Abcam, Cambridge, UK) and mouse primary antibodies: anti-INCENP at 1:1,000 (42), anti-human TOP2A at 1:200 (8D2, Medical & Biological Laboratories Co. Ltd., Nagoya, Japan), anti-BAZ1B at 1:100 (ab50987; Abcam), and anti-GAPDH at 1:10,000 (GTX627408; GeneTex Inc., San Antonio, TX, USA). IRDye 800CW donkey

anti-rabbit IgG at 1:15,000 (926-32211; Li-COR Biosciences, Lincoln, NE, USA) and anti-mouse IgG at 1:15,000 (926-32210; Li-COR Biosciences) were used as secondary antibodies. Immune complexes were detected using an Odyssey CLx Infrared Imaging System (Li-COR Biosciences) and visualized using Image Studio 5.2 (Li-COR Biosciences).

Time-lapse fluorescence microscopy

Wild type (WT) or BAZ1B knockout (KO) HeLa cells were transfected with the histone H2B-mRFP fusion protein expression plasmid pRFP-C-H2B using Lipofectamine LTX. Stable cell clones expressing the fusion protein were generated and maintained in DMEM with 10% FBS, 100 U/mL penicillin, 100 μg/mL streptomycin, and 400 μg/mL G418 (074-05963; Wako Pure Chemical Industries Ltd.) at 37°C in a 5% CO_2 atmosphere. For capturing images, cells were grown in 10% FBS-containing DMEM without phenol red (044-32955; Wako Pure Chemical Industries Ltd.). Time-lapse images were acquired every 5 min in a 5% CO_2/37°C chamber using a BioStation IM system (Nikon, Tokyo, Japan).

Drug treatment

Monastrol (M8515, Sigma), MG132 (474790, Merck, Kenilworth, NJ, USA), and RO-3306 (217721, Merck) were dissolved in DMSO and applied to cells at final concentrations of 5 μM, 9 μM, and 68 μM for 45 min, 20 h, and 4 h, respectively. To release RO-3306 or monastrol, cells arrested by inhibitors were switched to inhibitor-free medium after washing in this medium three times.

Cell cycle analysis

HeLa cells fixed in 4% paraformaldehyde (30525-89-4, Wako Pure Chemical Industries Ltd.) were probed with an anti-histone H3 S10ph antibody (1:3,000; D2C8, Cell Signaling Technology Inc., Danvers, MA, USA) and anti-α-tubulin antibody (1:5,000; B-5-1-2, Sigma-Aldrich) and then with Alexa-conjugated secondary antibodies; DNA was counterstained with 0.1 μg/mL DAPI. Mitotic cells were identified as histone H3 S10ph-positive cells and classified according to chromosomal morphology.

Mitotic chromosome spread

The cytospin technique was used to make chromosome spreads with preserved chromosome structure. Briefly, mitotic cells were synchronized by 0.1 μg/mL nocodazole treatment for 12 h and collected by tapping culture dishes. Cells were then treated with 75 mM KCl at 37°C for 15 min, and 10,000 cells were deposited onto coverslips by centrifugation at 800 rpm for 3 min.

Indirect immunofluorescence microscopy

After fixing for 7 min in 4% paraformaldehyde, cells were blocked with 1% (v/v) BSA in PBS and probed with the following antibodies: anti-Ki-67 at 1:1,000 (D3B5, Cell Signaling Technology Inc.), anti-NCAP-G at 1:1,000 (gift from Dr. Hirota), anti-CAP-H2 at 1:1,000 (CE-024A, Cosmo Bio Co. Ltd., Tokyo, Japan), and anti-TOP2A at 1:1,000 (8D2, Medical & Biological Laboratories Co. Ltd.). Cells were washed three times with PBS for 5 min before adding Alexa-conjugated secondary antibodies (Thermo Fisher Scientific) at 1:600; DNA was counterstained with 0.1 μg/mL DAPI.

Quantitative proteomics of the mitotic chromosome scaffold

Single focal plane images were obtained under an Olympus FV1000 microscope (IX81 confocal microscope system with a UPlan SApo 60×/1.35 oil-immersion objective lens; Olympus, Tokyo, Japan). FV10-ASW2.1 was used for visualization (Olympus), and images were Kalman-filtered to reduce noise.

Experimental design and statistical rationale

Mitotic chromosomes were isolated from chicken cells or human cells treated with nocodazole after six cell divisions to incorporate labeled arginine and lysine. Each sample for MS analysis was generated by combining three individual preparations of isolated mitotic chromosomes or mitotic chromosome scaffolds; two biological replicates for each cell type were analyzed. LC-MS/MS data were searched against UniProt database using MaxQuant 1.5.6.5 and statistically evaluated using one sample test in Perseus 1.6.1.3 (43). Continuous variables were expressed as the mean ± SD, variance was evaluated by F-test, and the significance of the results was analyzed by Welch's *t*-test in R. Differences were considered significant at $p \leq 0.05$.

RESULTS

Protein composition of the mitotic chromosome scaffold

Previously, we reported that SILAC ratios were useful for distinguishing chromosomal protein classes (30). Here, we demonstrated their utility for identifying chromosome scaffold proteins. It was shown that mitotic chromosome scaffold proteins such as ScI (TOP2A) and ScII (SMC2) were accumulated in the fraction of histone-depleted mitotic chromosomes (29) and that the addition of 1% β-mercaptoethanol dissociated the chromosome scaffold (Fig. 1A) (2, 29). Therefore, to obtain accurate results, we compared proteins in the isolated scaffold with those in the background obtained by chromosome scaffold isolation with 1% β-mercaptoethanol. This procedure allowed removal of many contaminating proteins from the list of putative chromosome scaffold proteins (forward [FW] label: lysine-8 and arginine-10 [heavy] – chromosome scaffold; lysine-0 and arginine-0 [light] – background; Fig. S1A–D).

To examine reproducibility of the results, we used the same strategy with alternative labeling (reverse [RV] label: heavy – background, light – chromosome

scaffold). Accordingly, 786 proteins could be quantified more than once in the FW and RV labeling experiments. Labeling revealed that TOP2A, KIF4A, condensin subunits, PLK1 (a condensation regulation factor localized to the chromosome axis) (44), and BAZ1B were highly concentrated in the mitotic chromosome scaffold fraction (Fig. 1B, Table S3).

Proteins enriched in the mitotic chromosome scaffold versus mitotic chromosomes

We expected that core components of the chromosome scaffold, such as TOP2A and SMC2, should be more concentrated in the mitotic chromosome scaffold (insoluble) fraction compared to the soluble fraction from which the chromosome scaffold was removed. Therefore, we combined histone-depleted mitotic chromosomes from DT40 cells grown in heavy SILAC medium with an equal protein amount of the soluble fraction from a parallel culture grown in light SILAC medium (FW label; RV labeling was performed to investigate reproducibility; Fig. 1A, S1E). As a result, 739 proteins could be quantified more than once in the FW and RV

experiments. Ranking these proteins according to their enrichment in the chromosome scaffold fraction revealed that not only condensin subunits and TOP2A but also several centromere/kinetochore proteins were enriched in the chromosome scaffold, whereas condensin II subunits were less abundant (Fig. 1C). Furthermore, BAZ1B was as enriched as other scaffold components in histone-depleted mitotic chromosomes (Fig. 1C). Interestingly, even core histones were not observed in the histone-depleted mitotic chromosome fraction (Fig. 1A, C); however, we detected anomalous levels of histone macroH2A (Fig. 1C, S1F), which could possibly be involved in linking histones and chromosome scaffolds during chromosome condensation.

Protein composition in histone-depleted mitotic chromosomes of SMC2^{ON} and SMC2^{OFF} cells

SMC2 is essential for the formation of the mitotic chromosome scaffold (11). Therefore, we used the histone-depleted mitotic chromosome fraction isolated from SMC2 KO cells as a possible second background fraction. Previously, we compared

protein composition in mitotic chromosomes of SMC2^{ON} and SMC2^{OFF} cells (45). Here, we assessed protein abundance in histone-depleted mitotic chromosomes obtained from cells expressing SMC2 or not. For this, we combined equal amounts of histone-depleted mitotic chromosomes isolated from SMC2^{ON} cells in heavy SILAC medium and SMC2^{OFF} cells in light SILAC medium (Fig. S2A). Consistent with the results of the previous experiment, TOP2A, KIF4A, and condensin subunits were not concentrated in histone-depleted mitotic chromosomes from SMC2^{OFF} cells; however, BAZ1B was concentrated (Fig. S2B, C). This finding suggests that, unlike other scaffold proteins, BAZ1B associates with the chromosome scaffold independently of condensin.

BAZ1B localizes to the mitotic chromosome axis

To validate our quantitative proteomic data, we isolated histone-depleted mitotic chromosomes (chromosome scaffolds) from HeLa cells and assessed the levels of BAZ1B by immunoblotting (Fig. 1D). Furthermore, to ensure that important protein mechanisms were conserved, we expressed GFP-tagged human BAZ1B in human epithelial U2OS cells and assessed its localization during mitosis. A previous study

showed localization of GFP-tagged condensin subunits SMC2-GFP, CAP-H:GFP, and CAP-D:GFP to the chromosome axis (18). In the control experiment, GFP-β-glucuronidase did not show any specific localization on mitotic chromosomes (Fig. 1E), whereas GFP-BAZ1B was confirmed to be localized to the chromosome axis (Fig. 1F), strongly suggesting that BAZ1B is associated with the chromosome scaffold during mitosis. Moreover, GFP signals were stronger in the centromeric and telomeric regions on the chromosome axis (Fig. 1F), indicating that BAZ1B localizes preferentially to the heterochromatin region.

BAZ1 deficiency alters progression through mitosis

To investigate whether BAZ1B plays a functional role in mitotic chromosomes, we generated mutant BAZ1B KO HeLa cells using CRISPR/Cas9; the lack of endogenous BAZ1B was confirmed by immunoblotting and DNA sequencing (Fig. 2A, S3A). Compared to WT cells, BAZ1B KO cells grew only slightly slower (Fig. 2B, S3B), which prompted us to investigate why BAZ1B KO cells were not more affected despite the known localization of BAZ1B to the chromosome axis. For this, we examined the

role of BAZ1B homolog BAZ1A by generating BAZ1A KO cells and BAZ1A/BAZ1B double-KO cells lacking endogenous BAZ1A or both BAZ1 proteins, respectively (Fig. 2A, S3C). BAZ1 and BAZ1B share the same structure and interact with each other and with SMARCA5 (21, 46); however, BAZ1A has two instead of three WSTF-HB1-Itc1p-MBD9 (WHIM) DNA-binding domains (Fig. 2C). Similar to BAZ1B, GFP-BAZ1A was confirmed to be present in the nuclei in interphase (Fig. S4A, B), but it was difficult to detect its localization to the chromosomes and chromosomal axis in mitosis (Fig. S4C). Nonetheless, immunoblotting clearly showed that BAZ1A existed in isolated mitotic chromosomes but not in chromosome scaffolds (Fig. 1D). BAZ1A KO and WT cells exhibited similar growth; however, BAZ1A/B double-KO cells grew significantly slower than WT cells, but GFP-BAZ1B overexpression partially restored normal growth in double-KO cells (Fig. 2B, S3B). Mitotic profiles revealed that the percentage of cells at prometaphase tended to be higher in the double-KO group (47%) compared to the WT group (37%); at the same time, the proportion of cells at anaphase and telophase decreased in the double-KO group compared to the WT group (7% versus 13% in anaphase and 9% versus 15% in telophase, respectively;

Fig. 2D). However, GFP-BAZ1B overexpression partially restored segregation in double-KO cells (Fig. 2D). On the other hand, BAZ1A KO or BAZ1B KO cells did not show significant changes in the mitotic profile compared to WT cells (Fig. 2D). Therefore, to focus on the delay of chromosome alignment in double-KO cells, we next analyzed prometaphase arrest by synchronizing cells at the prometaphase stage by monastrol treatment for 4 h and then placing them into monastrol-free medium supplemented with MG132. Monastrol treatment led to the arrest of approximately 15% of total cells that were in mitosis, 80% of which were in early prometaphase (Fig. 2E). However, after 1 h in monastrol-free medium, the percentages of BAZ1B KO and BAZ1A/B double-KO cells in early prometaphase were significantly higher compared to that of WT cells (42% and 56% versus 21%, respectively), whereas the percentages of cells in metaphase were significantly lower (31% and 17% versus 63%, respectively; Fig. 2E). At the same time, no significant differences were observed between BAZ1A KO and WT cells (Fig. 2E). These results suggest that although BAZ1B is important for mitosis progression, endogenous BAZ1A alleviates the BAZ1B KO phenotype, whereas BAZ1A/B double-KO aggravates it.

Quantitative proteomics of the mitotic chromosome scaffold

Segregation errors were detected in less than 6% of WT, BAZ1A KO, and BAZ1B KO cells but in 15% of double-KO cells (Fig. 2F, G); however, GFP-BAZ1B overexpression partially restored segregation in double-KO cells (Fig. 2F). It has been shown that segregation errors are frequently observed in cells deficient in condensin I or II, which are localized to the mitotic chromosome axis (13, 47, 48), suggesting that BAZ1 proteins may perform a similar function. Furthermore, time-lapse imaging of histone H2B-mRFP-expressing cells showed a slight increase in the time between estimated NEB and anaphase onset in double-KO cells (33.8 min) compared to WT, BAZ1A KO, and BAZ1B KO cells (28.6, 29.8, and 29.4 min, respectively; Fig. 2H, I and Supplemental movie 1–5). Furthermore, double-KO cells showed a significant increase in segregation errors at anaphase compared to WT cells (22.6% versus 1.5%, respectively; Fig. 2I, J).

Interestingly, the percentage of double-KO cells in prophase increased significantly following monastrol treatment, which was also observed in non-synchronized cells (Fig. 2D, E), although the difference was not significant.

Quantitative proteomics of the mitotic chromosome scaffold

BAZ1 deficiency causes mitotic entry delay

We further investigated the prophase delay in BAZ1A/B double-KO cells by immunofluorescence using the anti-histone H3 phospho-serine 10 (H3pS10) antibody and DAPI to visualize chromosome morphology before NEB. However, phosphorylation of histone H3 occurs and is completed in the preceding prophase (49, 50). Therefore, it should be noted that two types of chromosome morphology could be present in prophase in this study: relaxed chromosomes marking early prophase and condensed chromosomes marking late prophase (Fig. 3A-C). Late prophase, in which individual condensed chromosomes could be clearly recognized, was distinguishable from early prophase; however, about 34% of cells had chromosomes of both types, marking the third type: middle prophase (Fig. 3A-C). The percentage of WT cells in early prophase (36%) was lower, whereas that in late prophase (30%) was significantly higher compared with those of BAZ1A/B double-KO cells (58% and 18%, respectively), and a similar tendency was observed for BAZ1B KO cells (Fig. 3D).

We then investigated whether prophase delay occurred in synchronized cells.

Quantitative proteomics of the mitotic chromosome scaffold

WT or KO cells were arrested in the G2 phase using the Cdk 1 inhibitor RO-3306 (51), and prophase profiles were observed 10, 20, or 30 min after switching to RO-3306-free medium. At 10 min, 90% of all cells were in early prophase; however, at 20 and 30 min, there were significantly more cells at early prophase in BAZ1B KO or BAZ1A/B KO groups compared to WT (Fig. 3E). At the same time, there were significantly fewer cells in middle prophase for the BAZ1A/B KO group and in late prophase for both BAZ1A/B KO and BAZ1B KO groups compared to WT at 30 min after RO-3306 release (Fig. 3E). These results indicate that the absence of BAZ1B delays chromosome condensation onset, and the effect is further aggravated if BAZ1A is absent as well, suggesting that BAZ1A and BAZ1B might co-regulate the chromosomal condensation timing at early prophase.

Proteomics analysis of mitotic chromosomes lacking BAZ1 proteins

To further elucidate the role of BAZ1 in mitotic chromosomes, we compared the association of all chromosomal proteins with mitotic chromosomes in cells with and without BAZ1B or BAZ1A/B using our previously developed quantitative

proteomic approach (30, 52, 53). Mitotic chromosomes were isolated after mixing equal amounts of WT cells cultured with lysine-8 and arginine-10 (heavy) and BAZ1B KO or BAZ1A/B double-KO cells cultured with lysine-0 and arginine-0 (light) (Fig. S5A), and their proteomes were analyzed by MS. A total of 1,243 and 1,290 proteins were identified based on comparison between WT and BAZ1B KO or BAZ1A/B double-KO cells, respectively, in two separate experiments.

The lack of BAZ1B decreased the association of SMARCA5 with mitotic chromosomes in BAZ1B KO cells to ~30% of that in WT (Fig. 4A). Given that SMARCA5 interacts with BAZ1B in the S phase, our results indicate that the SMARCA5-chromosome association depends on BAZ1B. Moreover, although topoisomerase I is part of the BAZ1B/SMARCA5 complex in the S phase (26), its association with mitotic chromosomes was unchanged in BAZ1B KO or BAZ1A/B double-KO cells compared to that in WT cells, suggesting that topoisomerase I associates with chromosomes through the BAZ1B/SMARCA5 complex independently of BAZ1B (Fig. 4A, B).

No dramatic changes were observed in the mitotic chromosome scaffold components (condensin I and II, TOP2A, and KIF4A) in BAZ1A/B double-KO cells (Fig.

4B), suggesting that their association with mitotic chromosomes does not depend on BAZ1 proteins. Ki-67, a component of the mitotic chromosome periphery and one of the most abundant proteins in mitotic chromosomes (30) that regulates their organization via interaction with protein phosphatase 1 (PP1) (54), showed a tendency to decrease in BAZ1A/B double-KO cells compared with WT; however, the changes did not reach statistical significance in a volcano plot (Fig. 4B). Moreover, immunofluorescence staining with anti-Ki-67 antibodies did not reveal significant differences between WT and BAZ1A/B double-KO cells (Fig. 4C, D).

In addition, we analyzed protein phosphorylation in mitotic chromosomes by enriching for phosphopeptides using TiO_2-based HAMMOC (32, 55) and subjecting them to LC-MS/MS (Fig. S5A). In SILAC experiments comparing WT and BAZ1B KO cells or WT and BAZ1A/B double-KO cells, we identified 1,536 or 1,446 phosphorylation sites in proteins associated with isolated mitotic chromosomes, respectively. However, we were unable to identify phosphorylation sites directly targeted by BAZ1B or BAZ1A in mitotic chromosomes, even though the phosphorylation of chromosomal proteins was mildly reduced in BAZ1A/B double-KO

cells (Fig. S5B, C).

Mitotic chromosome axes remain intact in BAZ1A/B double-KO cells

Although the lack of BAZ1A/B resulted in a mild phenotype characterized by aberrant chromosome structure in prometaphase, we did not observe morphological abnormalities in mitotic KO cells after visualization of the chromosome axis and its components by immunofluorescence (Fig. 4E). Next, we quantified CAP-G, CAP-H2, and TOP2A in mitotic chromosome axes of KO cells relative to co-spread HeLa cells overexpressing histone H2B-mRFP fusion protein; the design of the experiment is shown in Fig. 4F. The presence of CAP-G and CAP-H2 was unchanged in all KO cells, whereas that of TOP2A tended to increase in double-KO cells compared to WT cells (Fig. 4G). These results suggest that BAZ1A and BAZ1B did not significantly affect chromosome axes in prometaphase.

To confirm a weak effect of BAZ1A and BAZ1B depletion on mitotic chromosome structure, we performed an intrinsic metaphase structure (IMS) assay (Fig. S6A-C), in which chromosome unfolding to 10-nm structures is induced by

removal of divalent cations, and then refolding is induced by Mg^{2+} addition (54, 56). Consistent with previous reports that mitotic chromosomes lacking SMC2 or KIF4A were severely impaired in the IMS assay even though they appeared morphologically normal (11, 18), we observed the same effect in chicken DT40 cells (Fig. S6B). Our experiment clearly showed that chromosomes in ~90% of BAZ1A or BAZ1B KO cells efficiently regained their normal morphology after the unfolding-refolding cycle (Fig. S6C), suggesting that BAZ1A and BAZ1B are not individually required for maintaining the intrinsic structure of mitotic chromosomes. Moreover, mitotic chromosomes lacking both BAZ1A and BAZ1B were slightly affected as evidenced by the fact that 80% of double-KO cells regained normal chromosome morphology, and GFP-BAZ1B transfection partially rescued this phenotype (Fig. S6C). The effect of BAZ1A/BAZ1B KO was significantly weaker compared to SMC2 KO in DT40 cells, suggesting that mitotic chromosomes retained their structure in synchronized prophase irrespectively of BAZ1A/B presence.

Discussion

Components of the chromosome scaffold play an important role in the formation of structurally stable mitotic chromosomes. In this study, we used MS to determine the protein composition of chromosome scaffolds in DT40 cells. Using quantitative proteomics, we identified proteins in the histone-depleted mitotic chromosome fraction, which were associated with the mitotic chromosome scaffold, including those not previously reported as scaffold components. One of them, BAZ1B, has been shown to serve as a transcription factor or tyrosine kinase (24, 25). Consistent with our findings, BAZ1B and BAZ1A were shown to be abundant in mitotic chromosomes assembled in *Xenopus* egg extracts (14, 28).

BAZ1B localization to chromosomal axes in mitosis confirmed the results of quantitative proteomics obtained herein. Although BAZ1B KO was not fatal, it decreased cell growth, and the effect was stronger for cells with double KO of BAZ1A and BAZ1B, suggesting that both BAZ1 proteins have similar functions. The chromosomal localization of GFP-tagged BAZ1A in mitosis was difficult to determine, but immunoblotting using isolated mitotic chromosomes clearly demonstrated

chromosomal association of endogenous BAZ1A in mitosis. However, BAZ1A/B double-KO cells did not exhibit a clear mitotic phenotype. In a cell-free system based on *Xenopus* egg extracts, depletion of SMARCA5/ISWI, which forms a complex with both BAZ1A and BAZ1B, affected nucleosome spacing but not chromosome assembly (28). This study suggested that the SMARCA5-BAZ1 complex enhances proper interactions between chromatin and proteins involved in mitotic chromosome structure by catalyzing their nucleosomal fluidity (28). Our results also revealed a longer duration between phosphorylation of H3pS10 in whole nuclei and complete chromosome condensation in BAZ1B KO or BAZ1A/B double-KO cells. Based on these findings, we propose a model in which BAZ1 proteins expeditiously enhance chromatin association of other chromosome scaffold proteins in early prophase by regulating nucleosome spacing. This model is supported by the localization of BAZ1A and BAZ1B to the nuclei before mitotic entry. However, our proteomic and immunofluorescence analyses suggest an independent association between BAZ1A/B and known chromosome scaffold proteins such as condensin, TOP2A, and KIF4. Thus, the lack of BAZ1A and BAZ1B caused chromosome condensation delay, which could be recovered

until prometaphase. These findings implied that the function of BAZ1 proteins involves regulation of proper chromosome condensation timing after phosphorylation of histone H3S10 rather than organizing mitotic chromosome structure; however, chromosome missegregation was detectable in BAZ1A and BAZ1B double-KO cells at the end of anaphase. BAZ1A/B double-KO cells demonstrated segregation errors in anaphase, which were similar to those reported in cells lacking condensin I or II (11, 13, 57). Moreover, IMS assay showed a slight increase in partially abnormal mitotic chromosome structure in prophase. This discrepancy suggested the possibility of an abnormality in mitotic chromosome structure of BAZ1A/B KO cells that was undetectable in this study.

We were unable to identify tyrosine residues whose phosphorylation levels were decreased in chromosomes of BAZ1B or BAZ1A/B KO cells using quantitative phosphoproteomics with HAMMOC, which is likely because of difficulties in detecting histone modifications by chromatin proteomics based on trypsin digestion (58). In future studies, putative histone phospho-tyrosine residues other than pTyr142 in H2A.X should be investigated. Further research should focus on the mechanisms

Quantitative proteomics of the mitotic chromosome scaffold

underlying phosphorylation-dependent regulation of mitotic chromosome segregation and BAZ1 control of chromosome condensation at mitotic entry through cooperation with other components in the mitotic chromosome scaffold.

References

1. Laemmli, U. K., Cheng, S. M., Adolph, K. W., Paulson, J. R., Brown, J. A., and Baumbach, W. R. (1978) Metaphase chromosome structure: the role of nonhistone proteins. *Cold Spring Harb. Symp. Quant. Biol.* 42 Pt 1, 351–360

2. Adolph, K. W., Cheng, S. M., and Laemmli, U. K. (1977) Role of nonhistone proteins in metaphase chromosome structure. *Cell* 12, 805–816

3. Taagepera, S., Rao, P. N., Drake, F. H., and Gorbsky, G. J. (1993) DNA topoisomerase II alpha is the major chromosome protein recognized by the mitotic phosphoprotein antibody MPM-2. *Proc Natl Acad Sci U S A* 90, 8407–8411

4. Earnshaw, W. C., and Heck, M. M. (1985) Localization of topoisomerase II in mitotic chromosomes. *J. Cell Biol.* 100, 1716–1725

5. Sikorav, J. L., and Jannink, G. (1994) Kinetics of chromosome condensation in the presence of topoisomerases: a phantom chain model. *Biophys. J.* 66, 827–837

6. Hirano, T., and Mitchison, T. J. (1994) A heterodimeric coiled-coil protein required for mitotic chromosome condensation in vitro. *Cell* 79, 449–458

7. Nishiwaki, T., Daigo, Y., Kawasoe, T., Nagasawa, Y., Ishiguro, H., Fujita, M., Furukawa, Y., and Nakamura, Y. (1999) Isolation and characterization of a human cDNA homologous to the Xenopus laevis XCAP-C gene belonging to the structural maintenance of chromosomes (SMC) family. *J. Hum. Genet.* 44, 197–202

8. Schmiesing, J. A., Ball, A. R., Gregson, H. C., Alderton, J. M., Zhou, S., and Yokomori, K. (1998) Identification of two distinct human SMC protein complexes involved in mitotic chromosome dynamics. *PNAS* 95, 12906–12911

9. Kimura, K., and Hirano, T. (1997) ATP-dependent positive supercoiling of DNA by 13S condensin: a biochemical implication for chromosome condensation. *Cell* 90, 625–634

10. Schmiesing, J. A., Gregson, H. C., Zhou, S., and Yokomori, K. (2000) A human condensin complex containing hCAP-C-hCAP-E and CNAP1, a homolog of Xenopus XCAP-D2, colocalizes with phosphorylated histone H3 during the early stage of mitotic chromosome condensation. *Mol. Cell. Biol.* 20, 6996–7006

11. Hudson, D. F., Vagnarelli, P., Gassmann, R., and Earnshaw, W. C. (2003) Condensin is required for nonhistone protein assembly and structural integrity of vertebrate mitotic chromosomes. *Dev. Cell* 5, 323–336

12. Ono, T., Losada, A., Hirano, M., Myers, M. P., Neuwald, A. F., and Hirano, T. (2003) Differential contributions of condensin I and condensin II to mitotic chromosome architecture in vertebrate cells. *Cell* 115, 109–121

13. Ono, T., Fang, Y., Spector, D. L., and Hirano, T. (2004) Spatial and temporal regulation of Condensins I and II in mitotic chromosome assembly in human cells. *Mol. Biol. Cell* 15, 3296–3308

14. Shintomi, K., Inoue, F., Watanabe, H., Ohsumi, K., Ohsugi, M., and Hirano, T. (2017) Mitotic chromosome assembly despite nucleosome depletion in Xenopus egg extracts. *Science* 356, 1284–1287

15. Shintomi, K., and Hirano, T. (2011) The relative ratio of condensin I to II determines chromosome shapes. *Genes Dev.* 25, 1464–1469

16. Wood, J. L., Liang, Y., Li, K., and Chen, J. (2008) Microcephalin/MCPH1 associates with the Condensin II complex to function in homologous recombination repair. *J Biol Chem* 283, 29586–29592

17. Maeshima, K., and Laemmli, U. K. (2003) A two-step scaffolding model for mitotic chromosome assembly. *Dev. Cell* 4, 467–480

18. Samejima, K., Samejima, I., Vagnarelli, P., Ogawa, H., Vargiu, G., Kelly, D. A., de Lima Alves, F., Kerr, A., Green, L. C., Hudson, D. F., Ohta, S., Cooke, C. A., Farr, C. J., Rappsilber, J., and Earnshaw, W. C. (2012) Mitotic chromosomes are

compacted laterally by KIF4 and condensin and axially by topoisomerase IIα. *J. Cell Biol.* 199, 755–770

19. Belmont, A. S., and Bruce, K. (1994) Visualization of G1 chromosomes: a folded, twisted, supercoiled chromonema model of interphase chromatid structure. *J. Cell Biol.* 127, 287–302

20. Bozhenok, L., Wade, P. A., and Varga-Weisz, P. (2002) WSTF-ISWI chromatin remodeling complex targets heterochromatic replication foci. *EMBO J.* 21, 2231–2241

21. Poot, R. A., Bozhenok, L., van den Berg, D. L. C., Steffensen, S., Ferreira, F., Grimaldi, M., Gilbert, N., Ferreira, J., and Varga-Weisz, P. D. (2004) The Williams syndrome transcription factor interacts with PCNA to target chromatin remodelling by ISWI to replication foci. *Nat Cell Biol* 6, 1236–1244

22. Lu, X., Meng, X., Morris, C. A., and Keating, M. T. (1998) A novel human gene, WSTF, is deleted in Williams syndrome. *Genomics* 54, 241–249

23. Culver-Cochran, A. E., and Chadwick, B. P. (2013) Loss of WSTF results in spontaneous fluctuations of heterochromatin formation and resolution, combined with substantial changes to gene expression. *BMC Genomics* 14, 740

24. Xiao, A., Li, H., Shechter, D., Ahn, S. H., Fabrizio, L. A., Erdjument-Bromage, H., Ishibe-Murakami, S., Wang, B., Tempst, P., Hofmann, K., Patel, D. J., Elledge, S. J., and Allis, C. D. (2009) WSTF regulates the H2A.X DNA damage response via a novel tyrosine kinase activity. *Nature* 457, 57–62

25. Cook, P. J., Ju, B. G., Telese, F., Wang, X., Glass, C. K., and Rosenfeld, M. G. (2009) Tyrosine dephosphorylation of H2AX modulates apoptosis and survival decisions. *Nature* 458, 591–596

26. Ribeyre, C., Zellweger, R., Chauvin, M., Bec, N., Larroque, C., Lopes, M., and Constantinou, A. (2016) Nascent DNA Proteomics Reveals a Chromatin Remodeler Required for Topoisomerase I Loading at Replication Forks. *Cell Rep*,

27. Lan, L., Ui, A., Nakajima, S., Hatakeyama, K., Hoshi, M., Watanabe, R., Janicki, S. M., Ogiwara, H., Kohno, T., Kanno, S.-I., and Yasui, A. (2010) The ACF1 complex is required for DNA double-strand break repair in human cells. *Mol. Cell* 40, 976–987

28. MacCallum, D. E., Losada, A., Kobayashi, R., and Hirano, T. (2002) ISWI remodeling complexes in Xenopus egg extracts: identification as major chromosomal components that are regulated by INCENP-aurora B. *Mol. Biol. Cell* 13, 25–39

29. Lewis, C. D., and Laemmli, U. K. (1982) Higher order metaphase chromosome structure: evidence for metalloprotein interactions. *Cell* 29, 171–181

30. Ohta, S., Bukowski-Wills, J.-C., Sanchez-Pulido, L., Alves, F. de L., Wood, L., Chen, Z. A., Platani, M., Fischer, L., Hudson, D. F., Ponting, C. P., Fukagawa, T., Earnshaw, W. C., and Rappsilber, J. (2010) The Protein Composition of Mitotic Chromosomes Determined Using Multiclassifier Combinatorial Proteomics. *Cell* 142, 810–821

31. Holt, L. J., Tuch, B. B., Villén, J., Johnson, A. D., Gygi, S. P., and Morgan, D. O. (2009) Global analysis of Cdk1 substrate phosphorylation sites provides insights into evolution. *Science* 325, 1682–1686

32. Masuda, T., Tomita, M., and Ishihama, Y. (2008) Phase transfer surfactant-aided trypsin digestion for membrane proteome analysis. *J. Proteome Res.* 7, 731–740

33. Rappsilber, J., Mann, M., and Ishihama, Y. (2007) Protocol for micro-purification, enrichment, pre-fractionation and storage of peptides for proteomics using StageTips. *Nat. Protocols* 2, 1896–1906

34. Maita, N., Tsukimura, T., Taniguchi, T., Saito, S., Ohno, K., Taniguchi, H., and Sakuraba, H. (2013) Human α-L-iduronidase uses its own N-glycan as a substrate-binding and catalytic module. *Proc Natl Acad Sci U S A* 110, 14628–14633

35. Cox, J., and Mann, M. (2008) MaxQuant enables high peptide identification rates, individualized p.p.b.-range mass accuracies and proteome-wide protein quantification. *Nat Biotech* 26, 1367–1372

36. Vizcaíno, J. A., Deutsch, E. W., Wang, R., Csordas, A., Reisinger, F., Ríos, D., Dianes, J. A., Sun, Z., Farrah, T., Bandeira, N., Binz, P.-A., Xenarios, I., Eisenacher, M., Mayer, G., Gatto, L., Campos, A., Chalkley, R. J., Kraus, H.-J., Albar, J. P., Martinez-Bartolomé, S., Apweiler, R., Omenn, G. S., Martens, L., Jones, A. R., and Hermjakob, H. (2014) ProteomeXchange provides globally coordinated proteomics data submission and dissemination. *Nat. Biotechnol.* 32, 223–226

37. Vizcaíno, J. A., Côté, R. G., Csordas, A., Dianes, J. A., Fabregat, A., Foster, J. M., Griss, J., Alpi, E., Birim, M., Contell, J., O'Kelly, G., Schoenegger, A., Ovelleiro, D., Pérez-Riverol, Y., Reisinger, F., Ríos, D., Wang, R., and Hermjakob, H. (2013) The PRoteomics IDEntifications (PRIDE) database and associated tools: status in 2013. *Nucleic Acids Res.* 41, D1063–9

38. Okuda, S., Watanabe, Y., Moriya, Y., Kawano, S., Yamamoto, T., Matsumoto, M., Takami, T., Kobayashi, D., Araki, N., Yoshizawa, A. C., Tabata, T., Sugiyama, N., Goto, S., and Ishihama, Y. (2017) jPOSTrepo: an international standard data repository for proteomes. *Nucleic Acids Res.* 45, D1107–D1111

39. Ohta, S., Hamada, M., Sato, N., and Toramoto, I. (2015) Polyglutamylated Tubulin Binding Protein C1orf96/CSAP Is Involved in Microtubule Stabilization in Mitotic Spindles. *PLoS ONE* 10, e0142798

40. Brinkman, E. K., Chen, T., Amendola, M., and van Steensel, B. (2014) Easy quantitative assessment of genome editing by sequence trace decomposition. *Nucleic Acids Res.* 42, e168

41. Hoffmann, A., Heck, M. M., Bordwell, B. J., Rothfield, N. F., and Earnshaw, W. C. (1989) Human autoantibody to topoisomerase II. *Exp. Cell Res.* 180, 409–418

42. Cooke, C. A., Heck, M. M., and Earnshaw, W. C. (1987) The inner centromere protein (INCENP) antigens: movement from inner centromere to midbody during mitosis. *J. Cell Biol.* 105, 2053–2067

43. Tyanova, S., Temu, T., Sinitcyn, P., Carlson, A., Hein, M. Y., Geiger, T., Mann, M., and Cox, J. (2016) The Perseus computational platform for comprehensive analysis of (prote)omics data. *Nat. Methods* 13, 731–740

44. Abe, Y., Sako, K., Takagaki, K., Hirayama, Y., Uchida, K. S. K., Herman, J. A., DeLuca, J. G., and Hirota, T. (2016) HP1-Assisted Aurora B Kinase Activity Prevents Chromosome Segregation Errors. *Dev. Cell* 36, 487–497

45. Ohta, S., Montaňo-Gutierrez, L. F., Alves, F. de L., Ogawa, H., Toramoto, I., Sato, N., Morrison, C. G., Takeda, S., Hudson, D. F., Rappsilber, J., and Earnshaw, W. C. (2016) Proteomics analysis with a nano Random Forest approach reveals novel functional interactions regulated by SMC complexes on mitotic chromosomes. *Mol. Cell Proteomics* 15, 2802–2818

46. Collins, N., Poot, R. A., Kukimoto, I., García-Jiménez, C., Dellaire, G., and Varga-Weisz, P. D. (2002) An ACF1–ISWI chromatin-remodeling complex is required for DNA replication through heterochromatin. *Nat. Genet.* 32, 627–632

47. Abe, S., Nagasaka, K., Hirayama, Y., Kozuka-Hata, H., Oyama, M., Aoyagi, Y., Obuse, C., and Hirota, T. (2011) The initial phase of chromosome condensation requires Cdk1-mediated phosphorylation of the CAP-D3 subunit of condensin II. *Genes Dev.* 25, 863–874

48. Gerlich, D., Hirota, T., Koch, B., Peters, J.-M., and Ellenberg, J. (2006) Condensin I stabilizes chromosomes mechanically through a dynamic interaction in live cells. *Curr. Biol.* 16, 333–344

49. Van Hooser, A., Goodrich, D. W., Allis, C. D., Brinkley, B. R., and Mancini, M. A. (1998) Histone H3 phosphorylation is required for the initiation, but not maintenance, of mammalian chromosome condensation. *J. Cell. Sci.* 111 (Pt 23), 3497–3506

50. Hendzel, M. J., Wei, Y., Mancini, M. A., Van Hooser, A., Ranalli, T., Brinkley, B. R., Bazett-Jones, D. P., and Allis, C. D. (1997) Mitosis-specific phosphorylation of histone H3 initiates primarily within pericentromeric heterochromatin during G2 and spreads in an ordered fashion coincident with mitotic chromosome condensation. *Chromosoma* 106, 348–360

51. Vassilev, L. T., Tovar, C., Chen, S., Knezevic, D., Zhao, X., Sun, H., Heimbrook, D. C., and Chen, L. (2006) Selective small-molecule inhibitor reveals critical mitotic functions of human CDK1. *PNAS* 103, 10660–10665

52. Ohta, S., Wood, L., Toramoto, I., Yagyu, K.-I., Fukagawa, T., and Earnshaw, W. C. (2015) CENP-32 is required to maintain centrosomal dominance in bipolar spindle assembly. *Mol. Biol. Cell* 26, 1225–1237

53. Ohta, S., Bukowski-Wills, J.-C., Wood, L., de Lima Alves, F., Chen, Z., Rappsilber, J., and Earnshaw, W. C. (2010) Proteomics of isolated mitotic chromosomes identifies the kinetochore protein Ska3/Rama1. *Cold Spring Harb. Symp. Quant. Biol.* 75, 433–438

54. Booth, D. G., Takagi, M., Sanchez-Pulido, L., Petfalski, E., Vargiu, G., Samejima, K., Imamoto, N., Ponting, C. P., Tollervey, D., Earnshaw, W. C., and Vagnarelli, P. (2014) Ki-67 is a PP1-interacting protein that organises the mitotic chromosome periphery. *Elife* 3, e01641

55. Sugiyama, N., Masuda, T., Shinoda, K., Nakamura, A., Tomita, M., and Ishihama, Y. (2007) Phosphopeptide enrichment by aliphatic hydroxy acid-modified metal oxide chromatography for nano-LC-MS/MS in proteomics applications. *Mol. Cell Proteomics* 6, 1103–1109

56. Earnshaw, W. C., and Laemmli, U. K. (1983) Architecture of metaphase chromosomes and chromosome scaffolds. *J. Cell Biol.* 96, 84–93

57. Green, L. C., Kalitsis, P., Chang, T. M., Cipetic, M., Kim, J. H., Marshall, O., Turnbull, L., Whitchurch, C. B., Vagnarelli, P., Samejima, K., Earnshaw, W. C.,

Choo, K. H. A., and Hudson, D. F. (2012) Contrasting roles of condensin I and condensin II in mitotic chromosome formation. *J. Cell. Sci.* 125, 1591–1604

58. Ohta, S., Kimura, M., Takagi, S., Toramoto, I., and Ishihama, Y. (2016) Identification of Mitosis-Specific Phosphorylation in Mitotic Chromosome-Associated Proteins. *J. Proteome Res.* 15, 3331–3341

59. Baker, P. R., and Chalkley, R. J. (2014) MS-viewer: a web-based spectral viewer for proteomics results. *Mol. Cell Proteomics* 13, 1392–1396

Acknowledgments

The authors thank Iyo Toramoto and Fusako Kawasaki (Kochi University) for her technical assistance. This work was supported by grants from the Kanae Foundation for the promotion of medical science and JSPS KAKENHI (Grant Number 16K18494) to SO, Joint Usage and Joint Research Programs, the Institute of Advanced Medical Sciences, Tokushima University to SO and HT, and the Wellcome Trust (103139 and 108504) to JR. The Wellcome Centre for Cell Biology is supported by core funding from the Wellcome Trust (203149).

Data Availability

Raw mass spectrometry data and identifying information were deposited in the ProteomeXchange Consortium (http://proteomecentral.proteomexchange.org) via the JPOST partner repository (dataset identifiers: PXD007269, PXD008429, and PXD008696). All annotated spectra can be viewed online using MS-Viewer program with the search keys: 8rglnldw7p (PXD007269/JPST000280), wknsdrblrg (PXD008429/JPST000371), eojwtwjpx9, abnmmamhki, 8hpzu14nmo, and dktflsemfp (PXD008696/JPST000281) (59).

Figure legends

Fig. 1. Proteomics of proteins concentrated in the mitotic chromosome scaffold. (A) Chromosomes, histone-depleted mitotic chromosomes, or histone-enriched (soluble) fraction isolated with (+) or without (-) 1% β-mercaptoethanol (βME) from DT40 cells were analyzed by immunoblotting using antibodies against SMC2, Top2A, or INCENP and Coomassie Brilliant Blue (CBB) staining for core histones. Each sample corresponded to the same number of isolated chromosomes. (B) Identification of 511 overlapped proteins in SILAC forward versus reverse labeling experiments comparing histone-depleted mitotic chromosomes isolated with and without βME addition. (C) Identification of 352 overlapped proteins in forward versus reverse labeling experiments comparing histone-depleted mitotic chromosomes and total mitotic chromosomes. (D) Chromosomes, histone-depleted mitotic chromosomes, or soluble fraction isolated with (+) or without (-) 1% βME from HeLa cells were analyzed by immunoblotting using antibodies against TOP2A, BAZ1B, or BAZ1A and by CBB staining. Each sample corresponded to the same number of isolated chromosomes. (E, F) GFP-β-glucuronidase (GFP-Gus, E) and GFP-BAZ1B (F)

were expressed in human epithelial U2OS cells and analyzed for intracellular localization; (a, b) metaphase and (c) anaphase. GFP-BAZ1B and GFP-Gus are shown in green, and DAPI-stained nuclei are red. Scale bars, 5 μm. High-magnification immunofluorescence images of white boxes are on the right.

Fig. 2. Characterization of BAZ1B knockout cells in mitosis. (A) Wild-type (WT), BAZ1A knockout (KO), BAZ1B KO, or BAZ1A/B double-KO cell extracts were analyzed by immunoblotting using antibodies against BAZ1A, BAZ1B, or GAPDH. (B) Doubling time of WT and KO cells and BAZ1B KO and BAZ1A/B double-KO cells expressing GFP-BAZ1B based on growth curves shown in Fig. S3A. (C) Subdomain comparison between BAZ1A and BAZ1B (WAC: WSTF/Acf1/cbpq46 domain; DTT: DNA-binding homeobox and different transcription factor motifs; W1, W2, or W3: WAKZ motif 1, 2, or 3, respectively; PHD: PHD zinc finger; BR: bromodomain). (D) Mitotic profiles of WT and KO cells; immunofluorescence images show chromosome morphology in each phase (blue, DAPI; green, histone H3pS10; red, α-tubulin). (E) Mitotic profiles of WT and KO cells treated with monastrol or MG132 after monastrol release. (F)

Frequency of chromosome missegregation in anaphase of WT and KO cells. (G) Chromosome missegregation in anaphase of BAZ1A/B double-KO cells. (H) Mitosis duration was measured as the time from estimated nuclear envelope breakdown (NEB) until anaphase onset based on time-lapse imaging data. (I) Time-lapse imaging of histone H2B-mRFP-expressing WT and KO cells. Green or pink arrowheads mark estimated NEB or anaphase onsets, respectively. Time from estimated NEB onset (0’) is shown. Yellow arrowheads mark bridged chromosomes. (J) Chromosome missegregation was quantified as the number of anaphase events with lagging or bridged chromosomes divided by the total number of anaphase events based on time-lapse images. All data are presented as the mean ± SD; *p < 0.05, **p < 0.01, and ***p < 0.005 calculated by Welch's *t*-test (n, number of repeated experiments; N, total sample number).

Fig. 3. Delay of chromosomal condensation timing in BAZ1A/B double-knockout cells in prophase. (A) Cartoon depicting changes in nuclear or chromosome morphology and phosphorylation level of H3pS10 (green) through

prophase determined in this study. (B, C) Three types of prophase chromosomes in wild-type (WT, B) and BAZ1A/B double-knockout (KO, C) cells. Histone H3 phosphorylated at Ser10 and DAPI-stained nuclei are shown. Scale bars, 5 μm. (D) Semi-quantitative analysis of the proportion of cells with prophase chromosome types shown in (A-C). (E) Semi-quantitative analysis of the proportion of cells with prophase chromosome types in WT and KO groups at 10, 20, or 30 min after RO-3306 release. The data are presented as the mean ± SD; *$p < 0.05$ and **$p < 0.01$; n.s., not significant (n, number of repeated experiments; N, total sample number).

Fig. 4 Effects of BAZ1 on mitotic chromosome structures. (A, B) Volcano plots of MS data comparing protein abundance ratios in mitotic chromosomes isolated from wild-type (WT) and BAZ1B knockout (KO) cells (A) and WT and BAZ1A/B double-KO cells (B). (C) Immunofluorescence images of WT and BAZ1A/B double-KO cells stained with Ki-67 antibodies and DAPI. High-magnification images of white boxes are presented on the right. Scale bar, 5 μm. (D) Quantification of Ki-67 presence on mitotic chromosomes of WT, BAZ1B KO, and BAZ1A/B double-KO cells based on

images shown in (C). Red lines represent average values. (E) Immunofluorescence images of WT, BAZ1A KO, BAZ1B KO, and BAZ1A/B double-KO cells stained with TOP2A and CAP-G antibodies and DAPI. High-magnification images of white boxes are presented on the right. Scale bar, 5 μm. (F) Strategy for quantification of chromosomal axis components using immunofluorescence staining. (G) Quantitative comparison of CAP-G, CAP-H2, and TOP2A presence in the mitotic chromosome axis of WT, BAZ1A KO, BAZ1B KO, and BAZ1A/B double-KO cells. The data are presented as the mean ± SD; n.s., not significant.

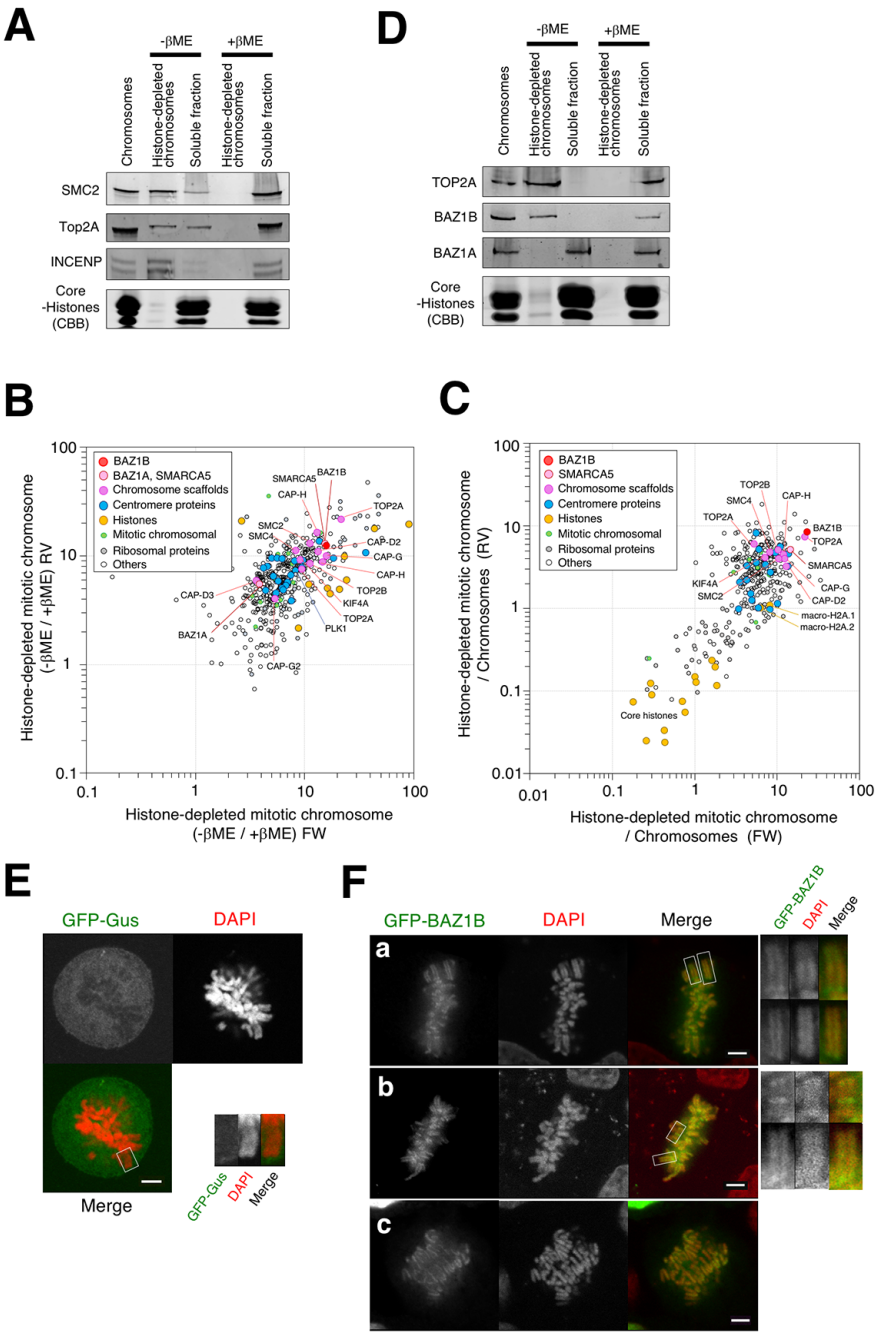
A
-βME
+βME
Chromosomes
Histone-depleted chromosomes
Soluble fraction
Histone-depleted chromosomes
Soluble fraction
SMC2
Top2A
INCENP
Core -Histones (CBB)
D
-βME
+βME
Chromosomes
Histone-depleted chromosomes
Soluble fraction
Histone-depleted chromosomes
Soluble fraction
TOP2A
BAZ1B
BAZ1A
Core -Histones (CBB)
B
BAZ1B
BAZ1A, SMARCA5
Chromosome scaffolds
Centromere proteins
Histones
Mitotic chromosomal
Ribosomal proteins
Others
Histone-depleted mitotic chromosome (-βME / +βME) RV
Histone-depleted mitotic chromosome (-βME / +βME) FW
C
BAZ1B
SMARCA5
Chromosome scaffolds
Centromere proteins
Histones
Mitotic chromosomal
Ribosomal proteins
Others
Histone-depleted mitotic chromosome / Chromosomes (RV)
Histone-depleted mitotic chromosome / Chromosomes (FW)
Core histones
E
GFP-Gus
DAPI
Merge
GFP-Gus
DAPI
Merge
F
GFP-BAZ1B
DAPI
Merge
GFP-BAZ1B
DAPI
Merge
a
b
c

Fig. 1

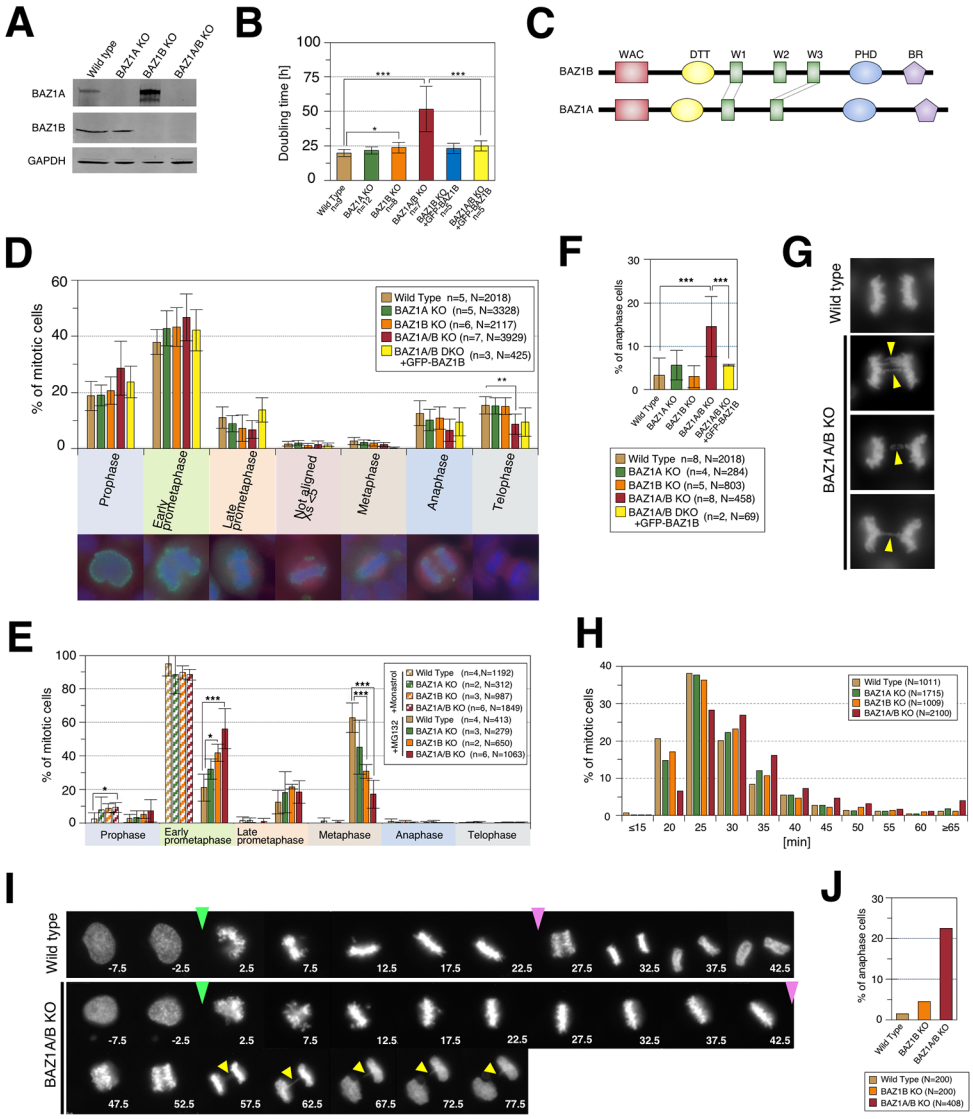
A
Wild type
BAZ1A KO
BAZ1B KO
BAZ1A/B KO
BAZ1A
BAZ1B
GAPDH
B
Doubling time [h]
C
WAC
DTT
W1
W2
W3
PHD
BR
BAZ1B
BAZ1A
D
% of mitotic cells
Wild Type n=5, N=2018)
BAZ1A KO (n=5, N=3328)
BAZ1B KO (n=6, N=2117)
BAZ1A/B KO (n=7, N=3929)
BAZ1A/B DKO (n=3, N=425) +GFP-BAZ1B
Prophase
Early prometaphase
Late prometaphase
Not aligned Xs
Metaphase
Anaphase
Telophase
F
% of anaphase cells
Wild Type n=8, N=2018)
BAZ1A KO (n=4, N=284)
BAZ1B KO (n=5, N=803)
BAZ1A/B KO (n=8, N=458)
BAZ1A/B DKO (n=2, N=69) +GFP-BAZ1B
G
Wild type
BAZ1A/B KO
E
% of mitotic cells
+Monastrol
+MG132
Wild Type (n=4,N=1192)
BAZ1A KO (n=2, N=312)
BAZ1B KO (n=3, N=987)
BAZ1A/B KO (n=6, N=1849)
Wild Type (n=4, N=413)
BAZ1A KO (n=3, N=279)
BAZ1B KO (n=2, N=650)
BAZ1A/B KO (n=6, N=1063)
H
% of mitotic cells
Wild Type (N=1011)
BAZ1A KO (N=1715)
BAZ1B KO (N=1009)
BAZ1A/B KO (N=2100)
[min]
I
Wild type
BAZ1A/B KO
J
% of anaphase cells
Wild Type (N=200)
BAZ1B KO (N=200)
BAZ1A/B KO (N=408)

Fig. 2

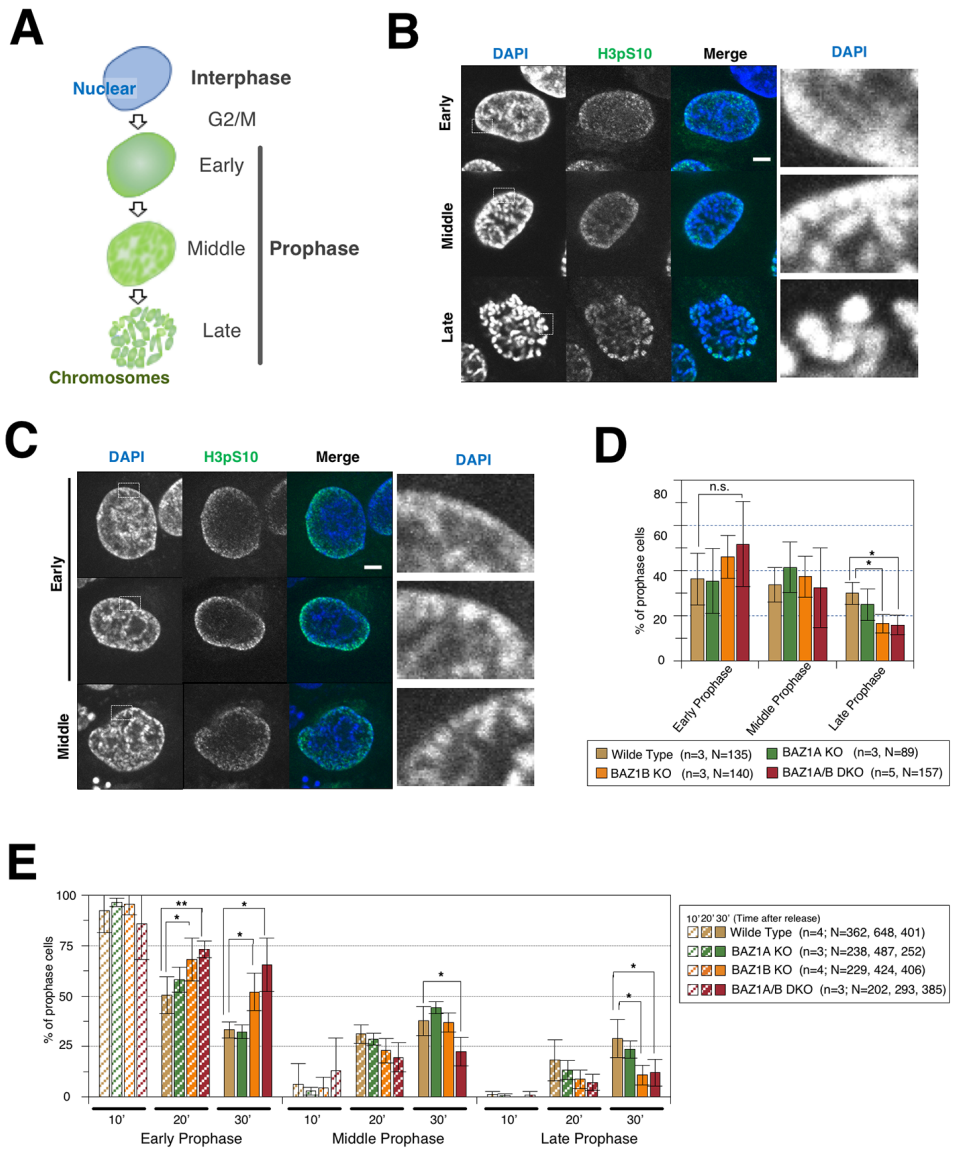
A
Nuclear
Interphase
G2/M
Early
Middle
Late
Prophase
Chromosomes
B
DAPI
H3pS10
Merge
DAPI
Early
Middle
Late
C
DAPI
H3pS10
Merge
DAPI
Early
Middle
D
n.s.
% of prophase cells
Early Prophase
Middle Prophase
Late Prophase
Wilde Type (n=3, N=135)
BAZ1A KO (n=3, N=89)
BAZ1B KO (n=3, N=140)
BAZ1A/B DKO (n=5, N=157)
E
% of prophase cells
10' 20' 30'
Early Prophase
Middle Prophase
Late Prophase
10'20'30' (Time after release)
Wilde Type (n=4; N=362, 648, 401)
BAZ1A KO (n=3; N=238, 487, 252)
BAZ1B KO (n=4; N=229, 424, 406)
BAZ1A/B DKO (n=3; N=202, 293, 385)

Fig. 3

Quantitative proteomics of the mitotic chromosome scaffold

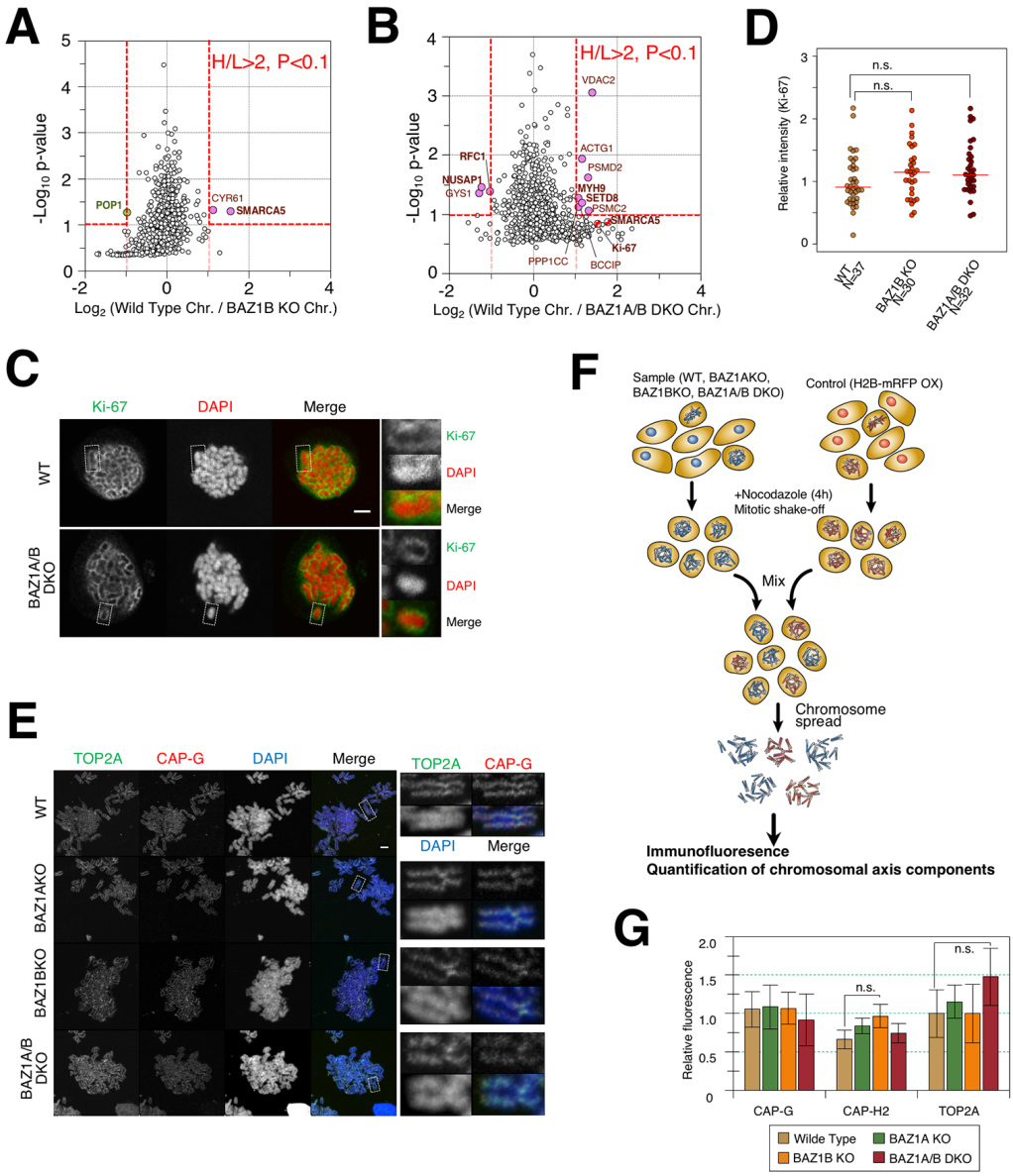

Fig. 4